Supporting Information

Composite Cluster-Organic Frameworks Based on Polyoxometalates and Copper/Cobalt-Oxygen Clusters

Xin-Xiong Li,[a] Chu-Chu Deng,[a] Dan Zhao,[b] Hao Yua,[a] Qing-Xin Zeng,*[a] and Shou-Tian Zheng*[a]

[a] *State Key Laboratory of Photocatalysis on Energy and Environment, College of Chemistry, Fuzhou University, Fuzhou, Fujian 350108, China.*

[b] *Fuqing Branch of Fujian Normal University, Fuqing, Fujian, 350300, China.*

Section 1: Experimental Section

Materials and General methods: All chemicals were commercially purchased and used without further purification. 2-(Hydroxymethyl)-2-(pyridin-4-yl)-1,3-propanediol (H_3L^a) and L-functionalized Anderson-type polyoxometalate $(TBA)_3MnMo_6O_{18}(L^a)_2\cdot 2CH_3CN$ were synthesized according to our previous work.[1] Elemental analyses of C, H and N were carried out with a Vario EL III elemental analyzer. Inductively coupled plasma (ICP) analyses were performed on a Jobin Yvon ultima2 spectrometer. IR spectra were recorded on an Opus Vertex 70 FT-IR infrared spectrophotometer in the range of 400 - 4000 cm^{-1}. Thermogravimetric analysis was performed on a Mettler Toledo TGA/SDTA 851e analyzer under an Ar-flow atmosphere with a heating rate of 10 ^oC/min in the temperature of 30 - 800 ^oC. Powder XRD patterns were obtained using a Rigaku DMAX 2500 diffractometer with CuKα radiation (λ = 1.54056 Å). Variable temperature susceptibility measurements were carried out in the temperature range 2 - 300 K at a magnetic field of 0.1 T on polycrystalline samples with a Quantum Design PPMS-9T magnetometer. The experimental susceptibilities were corrected for the Pascal's constants. Gas adsorption measurement was performed in the ASAP (Accelerated Surface Area and Porosimetry) 2020 System. Before measurement, **1** was activated by soaking the crystals in dichloromethane for three day to exchange NMF and 1,4-dioxane solvent molecules and then degassed at 333 K for 12 h under vacuum. Ac impedance measurements were carried out with a zennium/IM6 impedance analyzer over the frequency range from 0.1 Hz to 5 MHz with an applied voltage of 50mV. The relative humidity was controlled by a STIK Corp. CIHI-150B S3 incubator. The bulk conductivity was estimated by semicircle fittings of Nyquist plots.

Synthesis of $(CH_3NH_3)_3[Cu_4(\mu_3\text{-}O)_2(L^b)_4][MnMo_6O_{18}(L^a)_2]\cdot 4NMF\cdot 5H_2O$ (1): $CuBr_2$ (0.069 g, 0.309 mmol), $(TBA)_3MnMo_6O_{18}(L^a)_2\cdot 2CH_3CN$ (0.025 g, 0.012 mmol), 4-(2-(4-pyridyl)ethenyl) benzoic acid (0.025 g, 0.109 mmol) (L^b), tetrabutyl ammonium iodide (TBAI) (0.031 g, 0.084 mmol), N-methylformamide (NMF, 3 mL) and 1,4-dioxane (2 mL) were added respectively to a 20 mL vial, which was sealed and heated to 90 ^oC for 96 h, then cooled to room temperature. After washed by ethanol pure large pure green block crystals were obtained. Yield: 25 mg, ca. 72% based on $(TBA)_3MnMo_6O_{18}(L^a)_2\cdot 2CH_3CN$. Elemental analysis calcd (%) for $C_{85}H_{108}N_{13}O_{43}MnCu_4Mo_6$ (M_r = 2884.59): C, 35.39; H, 3.77; N, 6.31; Mn, 1.90; Cu, 8.81; Mo, 19.96. Found: C, 35.68; H, 3.62; N, 6.22; Mn, 1.83; Cu, 9.17; Mo, 20.76. IR (KBr, cm^{-1}): 3440(m), 3050(w), 2931(w), 2849(w),1605(vs), 1545(s), 1382(vs), 1215(w), 1176(w), 1069(m), 926(s), 846(w), 808(w), 781(w), 656(m), 623(w), 537(w), 466(w).

Synthesis of $[(CH_3)_2NH_2]_3[Co_5(\mu_3\text{-}O)_2(L^b)_6][MnMo_6O_{18}(L^a)_2]\cdot 5DMF$ (2): $Co(NO_3)_2\cdot 6H_2O$ (0.031 g, 0.106 mmol), $(TBA)_3MnMo_6O_{18}(L^a)_2\cdot 2CH_3CN$ (0.025 g, 0.012 mmol), 4-(2-(4-pyridyl)ethenyl)benzoic acid (0.015 g, 0.067 mmol), tetrabutyl ammonium iodide (TBAI) (0.020 g, 0.054 mmol), N,N-dimethylformamide (DMF, 3 mL) were added respectively to a 20 mL vial, which was sealed and heated to 90 ^oC for 96 h, then cooled to room temperature. After washed by N, N-dimethylformamide, pure large pure reddish brown block crystals were obtained. Yield: 21 mg, ca. 53% based on $(TBA)_3MnMo_6O_{18}(L^a)_2\cdot 2CH_3CN$. Elemental analysis calcd (%) for $H_{139}C_{123}N_{10}O_{43}MnCo_5Mo_6$ (M_r = 3370.70): C, 43.82; H, 4.16; N, 4.16; Mn, 1.63; Co, 8.74; Mo, 17.08. Found: C, 43.79; H, 4.20; N, 4.00; Mn, 1.51; Co, 8.25; Mo, 17.74. IR (KBr, cm^{-1}): 3434(m), 2930(w), 2855(w), 1659vs), 1599(vs), 1545(m), 1496(w), 1388(s), 1220(w), 1177(w), 1096(w), 1063(m), 922(s), 846(w), 815(w), 777(w), 663(s), 544(w), 441(w).

Synthetic considerations: In this work, we chose L^a, L^b and Anderson-type POM for exploration based on the following considerations: (1) As well known, Anderson-type POMs can be easily covelently grafted by tripodal alhocol ligands. The combination of L^a and Anderson-type POM would result in a linear rigid POM SBU $[MnMo_6O_{18}L^a{}_2]^{3-}$ which has been proved to be a good linker to join metal clusters due to the presence of two uncoordinated 4-pyridyl groups on its both sides. (2) L^b is a semi-rigid bifunctional ligand with a 4-pyridyl group and a carboxyl group on its two ends. The diverse functional groups make L^b together with $[MnMo_6O_{18}L^a{}_2]^{3-}$ to easily induce the transition-metal ions to form unique metal clusters *in situ*. Besides, owing to the flexible bridging ability, L^b can help $[MnMo_6O_{18}L^a{}_2]^{3-}$ clusters to join the *in situ* formed transition-metal clusters into extended structures effectively. As a result, composite cluster organic frameworks based on POM clusters and transition-metal clusters might be obtained.

Synthetic discussion: Generally, in a specific self-assembly process, many reaction parameters such as temperature, concentration, the reactant stoichiometric ratio and so on, have important influence on the formation of the final products. During our exploration, we found that the reactions are sensitive to reaction factors including the solvent, the auxiliary ligands, the transition-metal ions and extra non-reactive additive. First of all, the semi-rigid auxiliary ligand L^b is indispensable for the construction of **1** and **2**. Initially, we have tried a lot of times to assemble POM SBU $[MnMo_6O_{18}L^a{}_2]^{3-}$ with various divalent transition-metal ions directly. Unfortunately, we are fruitless. Even when semi-rigid L^b was replaced by rigid ligands such as 1, 4-dicarboxybenzene or 4,4'-biphenyldicarboxylic acid, no crystal was obtained. The possible reason is that the semi-rigid L^b is more flexible than 1, 4-dicarboxybenzene or 4, 4'-biphenyldicarboxylic acid in meeting the bridging requirement during the self-assembly process. Secondly, the self-assembly processes of **1** and **2** are sensitive to the solvents, and **1** and **2** can only formed in specific solvents. When DMF, DMA, DEF were used to instead of NMF, or 1,4-dioxane was removed from reaction system, **1** cannot be obtained. Also, when DMF was replaced by NMA, DEF, NMF, **2** disappeared. Thirdly, the transition-metal ions are another key factors in the construction of **1** and **2**. Previously, various divalent transition-metal ions such as Mn^{2+}, Co^{2+}, Ni^{2+}, Cu^{2+}, Zn^{2+}, Cd^{2+} have been introduced to the reaction system by us. However, we only obtained two structures. Finally, extra non-reactive additive tetrabutyl ammonium iodide (TBAI) was crucial for obtaining pure phases containing good quality crystals. During our experiments, we found that the crystal qualities can be improved distinctly when an appropriate amount of TBAI was added to the reaction system. If TBAI was removed from reaction system, the quality of crystals became poor. When the amount of TBAI was excess, no crystals formed.

Single-crystal structure analysis: Single-crystal X-ray diffraction data for **1-2** were collected on a Bruker APEX II diffractometer at 150 K equipped with a fine focus, 2.0 kW sealed tube X-ray source (MoK radiation, λ = 0.71073 Å) operating at 50 kV and 30 mA. The program SADABS was used for the absorption correction. The structures were solved by the direct method and refined on F^2 by full-matrix least-squares methods using the SHELXL-2013 program package. All hydrogen atoms attached to carbon atoms were generated geometrically. Due to the highly porous characteristic of structures, the charge compensation anions and guest solvent molecules cannot be definitely mapped by single-crystal X-ray diffractions. The residual electron density that could not sensibly be modeled as solvents or anions was removed via application of the SQUEEZE function in PLATON.[2] The final formulas of **1-2** were determined by the combination of single-crystal X-ray diffractions with the elemental analysis, thermogravimetric analysis and charge balance. Crystallographic data and structure refinements for **1** and **2** are summarized in Table S3. CCDC 1857896-1857897 contain supplementary crystallographic data for this paper. These data can be obtained free of charge from The Cambridge Crystallographic Data Centre via www.ccdc.cam.ac.uk/data_request/cif

Section 2: Tables

Table S1 The bond valence sum calculations for **1.**

Atoms	*Calcd for Cu^{I}*	*Calcd forCu^{II}*
Cu1	1.662	1.905
Cu2	1.594	1.957
Cu3	1.727	2.019
Cu4	1.597	1.920

Table S2 The bond valence sum calculations for **2.**

Atoms	*Calcd for Co^{II}*	*Calcd forCo^{III}*
Co1	1.949	1.992
Co2	2.113	2.140
Co3	2.214	2.243
Co4	2.113	2.141
Co5	2.227	2.259

Table S3 X-ray crystallographic data for **1-2**.

	1	**2**
Empirical formula	$C_{74}H_{60}O_{34}N_6Cu_4MnMo_6$	$C_{102}H_{80}O_{38}N_8Co_5MnMo_6$
Formula weight	2462.02	2950.97
Crystal system	Monoclinic	Monoclinic
Space group	*C2/c*	$P2_1/c$
a (Å)	23.454(5)	26.3211(11)
b (Å)	21.606(4)	22.8123(10)
c (Å)	25.214(5)	35.4863(14)
α	90	90
β	103.396(3)	105.266(4)
γ	90	90
V (Å^3)	12429(4)	20555.7(15)
Z	4	4
F(000)	4844	5856
ρcalcd (g cm^{-3})	1.316	0.954
Temperature (K)	175(2)	175(2)
μ(mm-1)	1.411	0.850
Refl. Collected	18344	173039
Independent relf.	10701	48846
Parameters	565	1360
GOF on F^2	1.010	0.897
Final R indices (I= 2σ(I))	$R_1= 0.0690$ $wR_2=0.1799$	$R_1= 0.0833$ $wR_2= 0.2047$
R indices (all data)	$R_1= 0.1104$ $wR_2= 0.1974$	$R_1= 0.1634$ $wR_2=0.2262$

$R_1 = \sum||F_o| - |F_c||/\sum|F_o|$. $wR_2 = [\sum w(F_o^2 - F_c^2)^2/\sum w(F_o^2)^2]^{1/2}$; $w = 1/[\sigma^2(F_o^2) + (xP)^2 + yP]$, $P = (F_o^2 + 2F_c^2)/3$, where x = 0.1127, y = 0 for **1**; x = 0.1093, y = 0 for **2**.

Section 3: Additional structural figures and characterizations

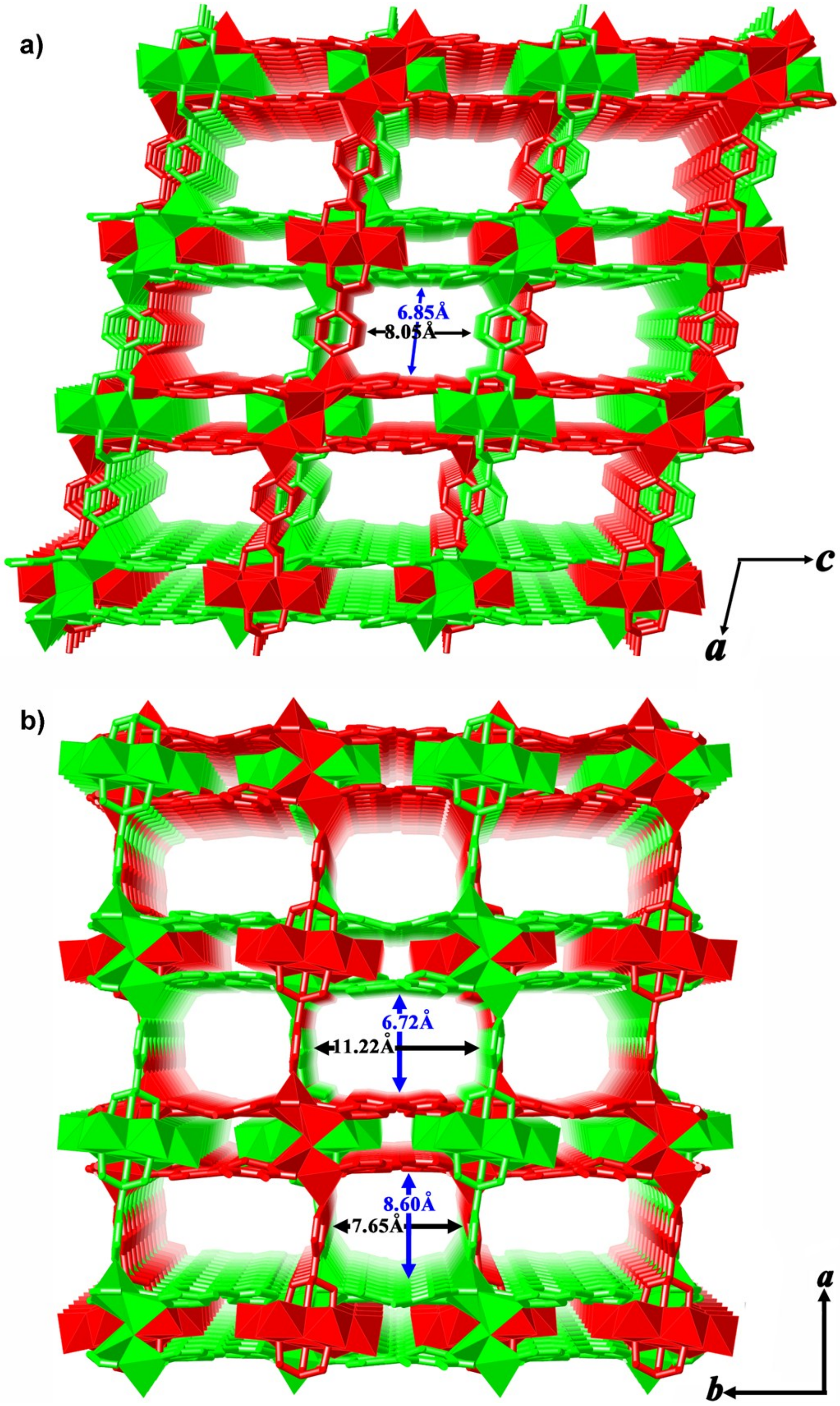

Figure S1. a) and b) View of the 2-fold interpenetrating ClusterOF of **1** along b-axis and c-axis, respectively.

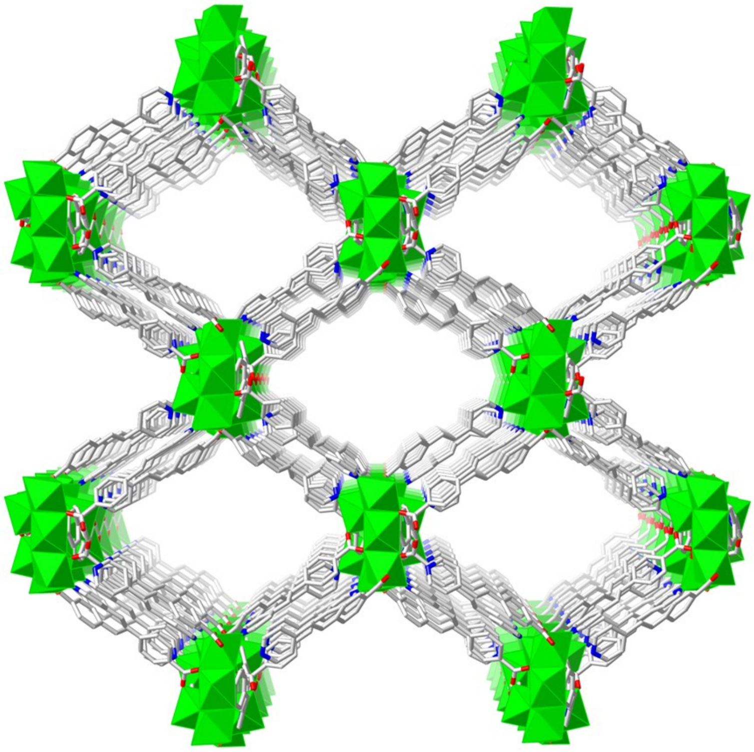

Figure S2. View of 3D Co_5-based ClusterOF of **2**. CoO_4N_2/CoO_6, green.

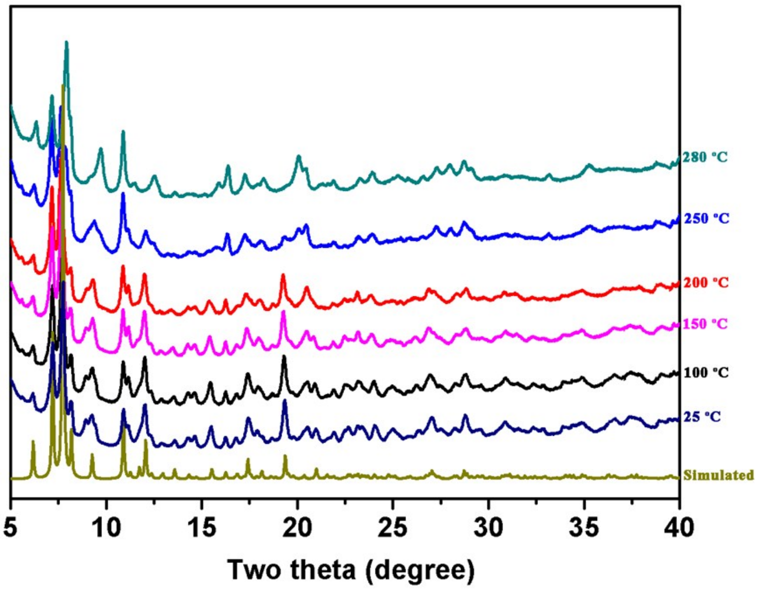

Figure S3. The simulated and variable-temperature PXRD patterns of **1**.

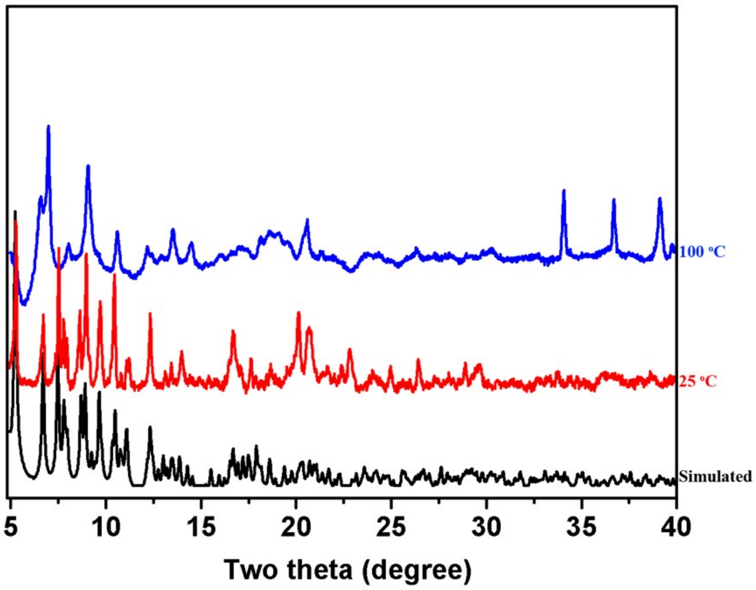

Figure S4. The simulated and variable-temperature PXRD patterns of **2**.

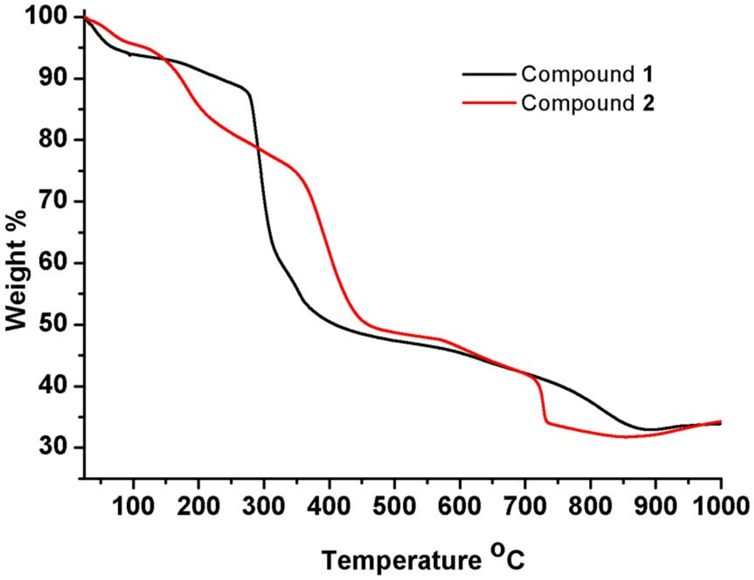

Figure S5. TGA curves of **1** and **2**.

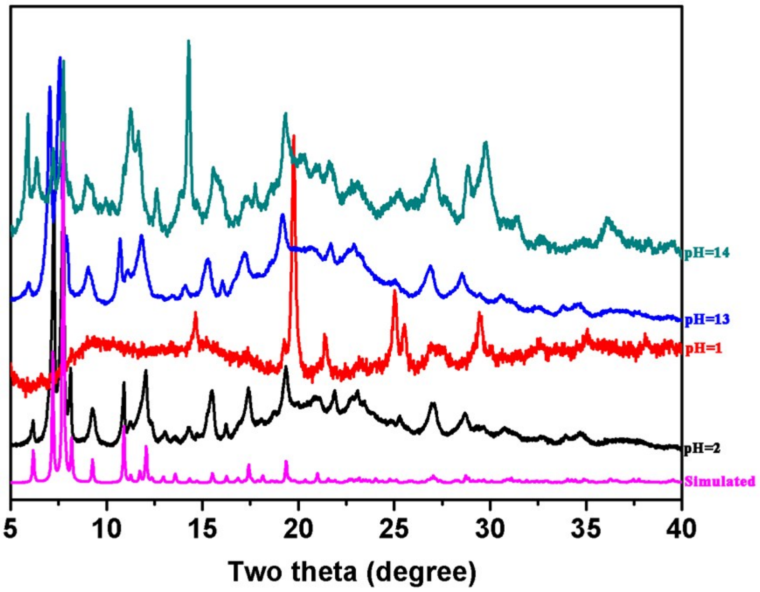

Figure S6. Simulated PXRD pattern of **1** and experimental patterns of as-synthesized **1** immersed in aqueous solution with different pH values.

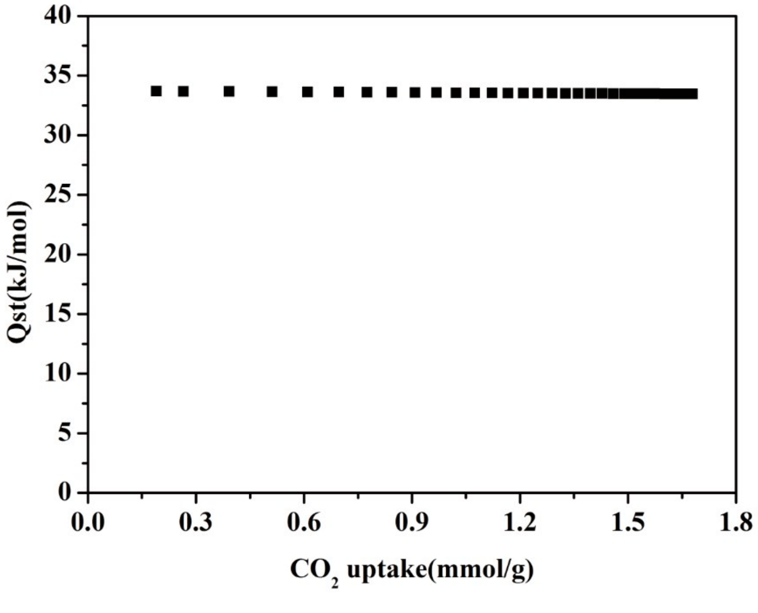

Figure S7. CO_2 adsorption enthalpies of **1**.

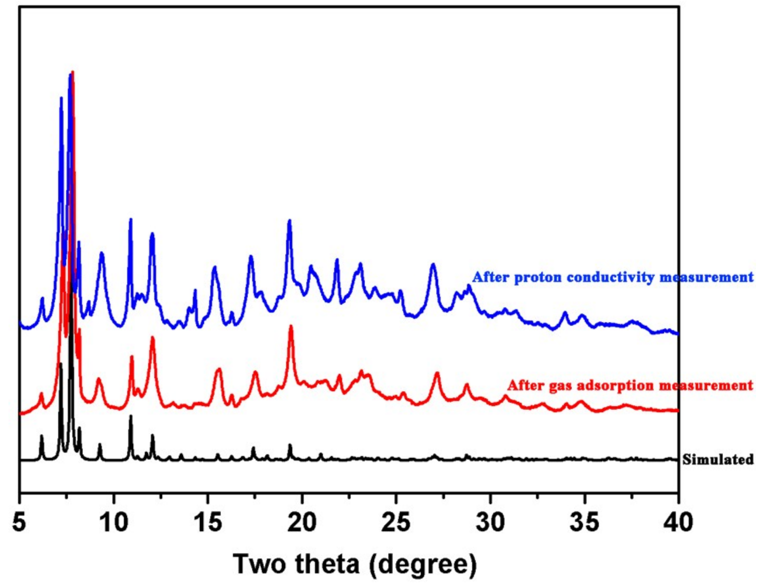

Figure S8. Simulated PXRD pattern of **1** and experimental patterns of **1** after gas adsorption and proton conductivity measurement.

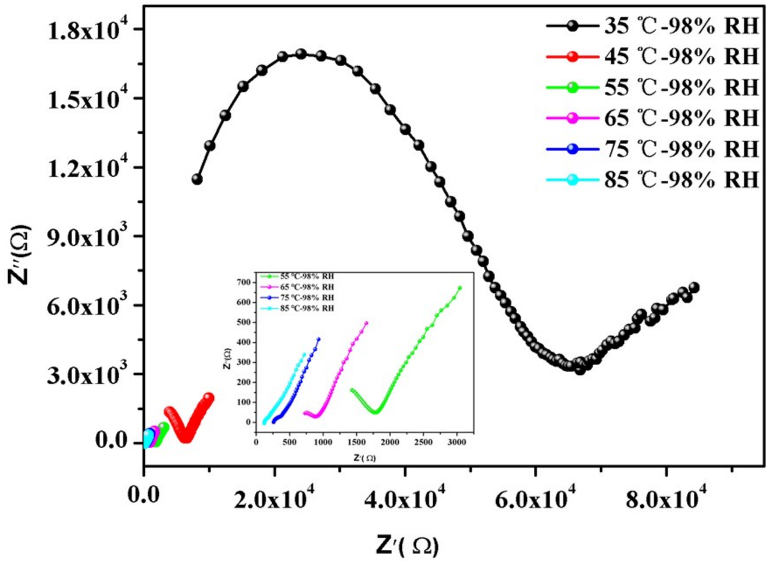

Figure S9. Nyquist plot of **1** under different temperatures with 98% RH.

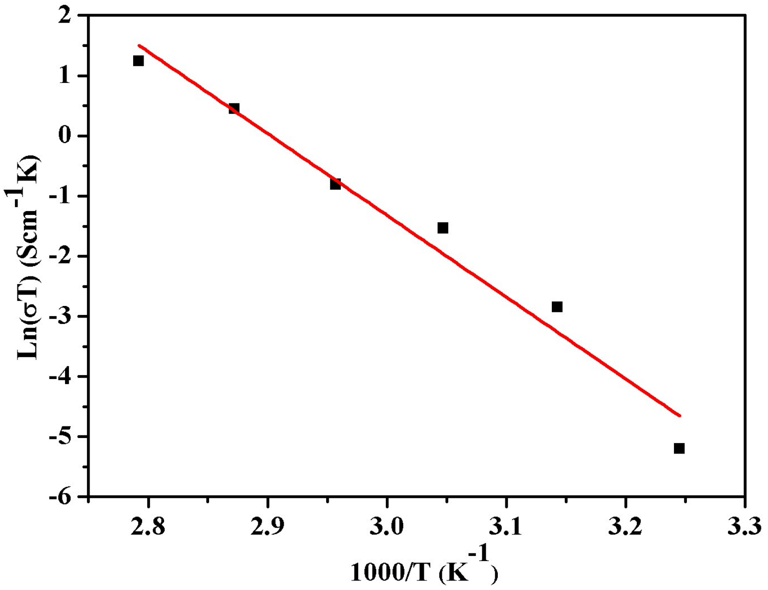

Figure S10 Arrhenius plots of the conductivity of **1**.

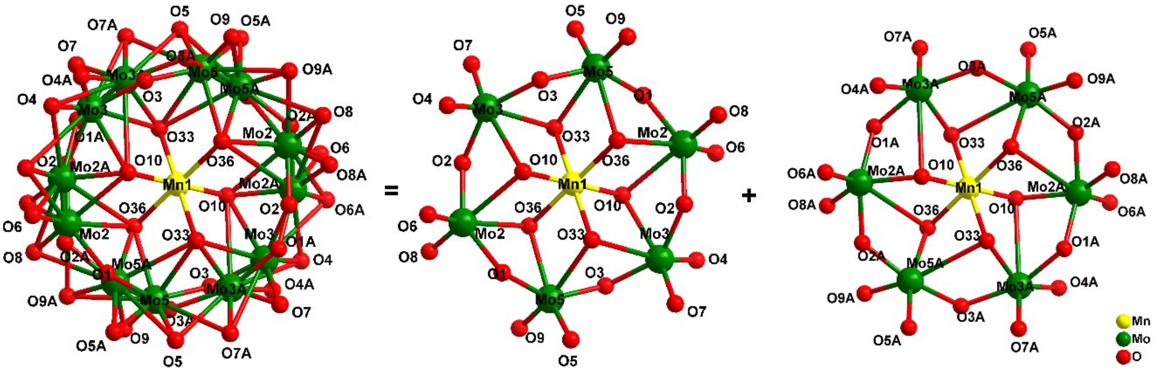

Figure S11. View of disordered model of the $\{MnMoO_{18}\}$ motif in compound **2**.

In **2**, the $\{MnMo_6O_{18}\}$ motif is found to be disordered and has been refined as a meaningful model by using PART. As shown in Figure S11, the $\{MnMo_6O_{18}\}$ motif is disordered into two sets with a free refined ratio of ca. 0.7/0.3. The ratio of disordered Mo atoms is then set to 0.7/0.3 according to their refined results. Within the disordered model, the six μ_2-O atoms between Mo atoms and the twelve terminal O atoms of Mo atoms are also disordered into two sites with the same ratio of 0.7/0.3.

Section 4: References

[1] X. X. Li, Y. X. Wang, R. H. Wang, C. Y. Cui, C. B. Tian, G. Y. Yang, *Angew. Chem. Int. Ed,* 2016, **55**, 6462.

[2] A. L. Spek, PLATON; Utrecht University: The Netherlands, 2003.